Hydrophilic Silver Nanoparticles Induce Selective Nanochannels in Thin Film Nanocomposite Polyamide Membranes

Zhe Yang,[a] Hao Guo,[a] Zhi-kan Yao,[a] Ying Mei[a] and Chuyang Y. Tang[a,b,c*]

[a] Department of Civil Engineering, the University of Hong Kong, Pokfulam, Hong Kong

[b] UNESCO Centre for Membrane Science and Technology, School of Chemical Engineering, University of New South Wales, Sydney, New South Wales 2052, Australia

[c] UNSW Water Research Centre, School of Civil and Environmental Engineering, University of New South Wales, Sydney, New South Wales 2052, Australia

[*] To whom all correspondence should be addressed.

Tel: +852 2859 1976, Fax: +852 2559 5337, E-mail address: tangc@hku.hk

ABSTRACT

Thin-film nanocomposite (TFN) membranes have been widely studied over the past decade for their desalination applications. For some cases, the incorporation of nonporous hydrophilic nanofillers has been reported to greatly enhance membrane separation performance, yet the underlying mechanism is poorly understood. The current study systematically investigates TFN membranes incorporated with silver nanoparticles (AgNPs). For the first time, we revealed the formation of nanochannels of approximately 2.5 nm in size around the AgNPs, which can be attributed to the hydrolysis of trimesoyl chloride monomers and thus the termination of interfacial polymerization by the water layer around each hydrophilic nanoparticle. These nanochannels nearly tripled the membrane water permeability for the optimal membrane. In addition, this membrane showed increased rejection against NaCl, boron, and a set of small-molecular organic compounds (e.g., propylparaben, norfloxacin, and ofloxacin), thanks to its combined effects of improved size exclusion, enhanced Donnan exclusion, and suppressed hydrophobic interaction. Our work provides fundamental insights into the formation and transport mechanisms involved in a solid-filler incorporated TFN membranes. Future studies should take advantage of this spontaneous nanochannel formation in the design of TFN for overcoming the classical membrane permeability-selectivity tradeoff.

TOC art

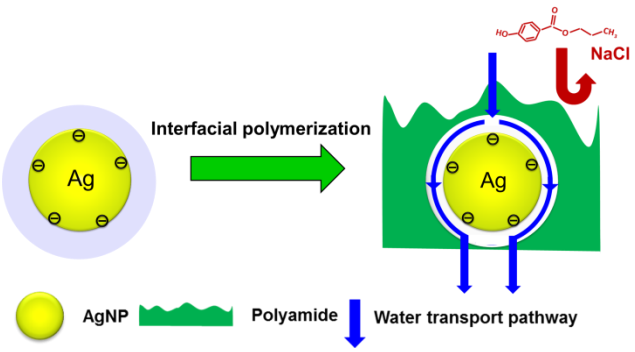
NaCl
Interfacial polymerization
Ag
Ag
AgNP
Polyamide
Water transport pathway

INTRODUCTION

Thin-film composite (TFC) polyamide membrane, formed by the interfacial polymerization (IP) reaction between *m*-phenylenediamine (MPD) and trimesoyl chloride (TMC),[1] is the core to reverse osmosis (RO) technology applied to seawater desalination wastewater reclamation.[2, 3] Its separation performance has a profound impact on the RO process.[1] Specifically, a membrane with high water permeability and selectivity can simultaneously decrease the specific energy consumptions and increase the permeance quality.[4] Unfortunately, the separation performance of commercial TFC RO membranes are constrained by the upper bound, a well-known tradeoff between membrane water permeability and selectivity.[5, 6] Thin-film nanocomposite (TFN) membrane that incorporates nanomaterials into the polyamide rejection layer is an effective strategy to overcome this permeability-selectivity tradeoff. In 2007, Hoek and co-workers[7] first reported the use of porous zeolite nanoparticles (NPs) to provide additional pathways to water in a polyamide rejection layer without compromising its salt rejection. After that, many other porous nanomaterials, such as mesoporous silica[8, 9], MOFs[10, 11], and aquaporins[12, 13] have been explored to enhance membrane separation performance.

In the last decade, researchers have also investigated the incorporation of solid nanofillers, such as silica,[14, 15] titanium dioxide,[16, 17] zinc oxide,[18, 19] cerium oxide,[20] , carbon quantum dots (CQDs),[21, 22] and silver nanoparticles (AgNPs)[23-25] to make TFN

membranes. Interestingly, many studies reported enhanced water permeability of their TFN membranes,[14-18] even though the nanomaterials contain no internal pores/channels. Researchers often attribute this flux enhancement to the hydrophilicity of the embedded nanofillers.[26] However, little is known about the nanoscale transport mechanism that leads to such enhancement. It is also worthwhile to note that several studies reported an opposite trend: decreased water fluxes upon the incorporation of solid nanofillers in TFN membranes.[12, 25, 27, 28] In addition to water flux, contradictory results related to salt rejection of solid nanofillers incorporated TFN membranes, either increased[23, 29] or declined,[27, 30, 31] have been reported (Table 1). Despite the dozens of papers published on this topic,[32] the apparently disparate phenomenological results prompt us to perform a systematic investigation on the underlying mechanism governing the transport in solid nanofillers incorporated TFN membranes.

In this study, we performed detailed characterization of TFN membranes incorporating AgNPs as nanofillers. Presumably, the highly hydrophilic nature of AgNPs can lead to the formation of a hydration layer around each nanoparticle ([33] and Figure 1a). With water molecules acting as terminators by hydrolyzing TMC, the presence of this water layer may prevent the formation of polyamide in the vicinity of the fillers. Therefore, we hypothesize that the addition of hydrophilic nanofillers into the aqueous MPD solution during interfacial polymerization induces the formation of

nanosized channels that facilitate water transport. For the first time, we provide compelling and direct microscopic evidence of the presence of nanochannels in an AgNPs-loaded TFN membrane. The role of these nanochannels on the transport of water, salt and micropollutants was systematically elucidated. Our study provides deep mechanistic insights for guiding the selection of nanofillers and design of TFN membranes.

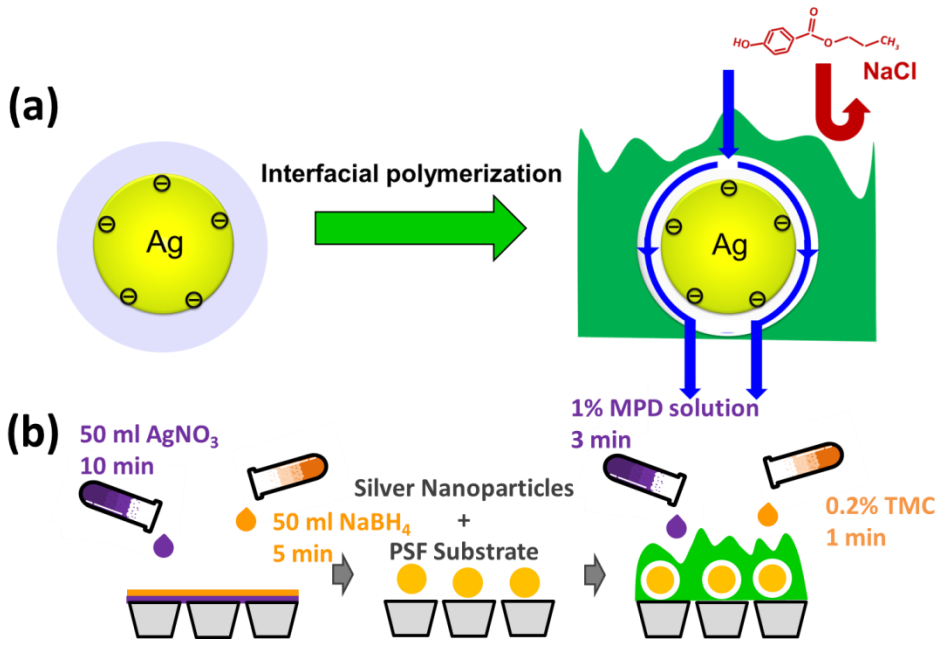

Figure 1. (a) Schematic diagram of the mechanism of AgNPs induced nanochannels in the polyamide layer for efficient water transport, (b) schematic diagram of membrane fabrication. A polysulfone substrate was soaked by 50 ml $AgNO_3$ solution and 50 ml $NaBH_4$ solution respectively to generate the AgNPs. Then, the interfacial polymerization reaction between 1% MPD and 0.2% TMC was performed on this AgNPs loaded substrate to obtain the final AgNPs incorporated TFN membranes.

MATERIALS AND METHODS

Materials and Chemicals. Unless specified otherwise, all reagents and chemicals were analytical grade and were purchased from Sigma-Aldrich. Polysulfone (PSF, Molecular weight ~35,000) and *N*,*N*-dimethylformamide (DMF, 99.8%, anhydrous) were used for preparing substrates. Silver nitrate ($AgNO_3$, ACS reagent, ≥99.0%) and sodium borohydride ($NaBH_4$, 98%) were applied to generate AgNPs. MPD (flakes, 99%), TMC(99%, J&K Scientific Ltd.) and hexane (HPLC grade, 95%) were used for synthesizing the polyamide rejection layer through interfacial polymerization reaction. Sodium chloride (NaCl) was purchased from Uni-Chem and boron, ethylene glycol, diethylene glycol, and pentaerythritol were obtained from Dieckmann Hong Kong. Propylparaben (99%, Mw 180.2, Acros Organics, Geel, Belgium), norfloxacin (NOR, Mw 319.3) and ofloxacin (OFL, Mw 361.4) were used as model trace organic contaminants (TrOCs). Propylparaben is an endocrine disrupting compounds, whereas both NOR and OFL are antibiotics.

Synthesis of Control PSF and AgNPs Coated PSF Substrates. Polysulfone (PSF) substrate was fabricated using a conventional phase inversion method following our previous work.[34] Due to their highly hydrophilic nature and ability to be easily generated *in situ* with minimized particle aggregation, AgNPs were used as model hydrophilic nanofillers in the current study.[35] AgNPs were generated *in situ* on the polysulfone substrate (Figure 1b) following the method reported in the literature.[35]

Briefly, a 50 ml $AgNO_3$ solution (1, 5, 20 or 100 mM) was poured onto a polysulfone substrate, and shaking was applied for 10 mins at 50 revolutions per minute (rpm). The extra $AgNO_3$ solution was removed. Then, a 50 ml $NaBH_4$ solution (with identical concentration to the $AgNO_3$ solution) was applied to the $AgNO_3$ soaked polysulfone substrate to reduce Ag^+ to AgNPs for 5 mins. The AgNPs-modified substrate was subsequently rinsed by deionized (DI) water for 5 mins and stored in DI water at 4 °C before use. The PSF substrates prepared in this study were named as PSF-Ag1, PSF-Ag5, PSF-Ag20 and PSF-Ag100 on the basis of the $AgNO_3$ concentration.

Synthesis of the TFC and TFC-Ag polyamide membranes. To obtain the TFC membrane, interfacial polymerization process was applied onto the control polysulfone and PSF-Ag substrates. Specifically, an AgNPs modified substrate was soaked in a 100 ml MPD/deionized (DI) water solution (1 wt%). The immersion time was set at 3 mins and extra MPD solution was removed. Then, a 25 ml TMC/hexane solution (0.2 wt%) was poured onto the polysulfone substrate with MPD to perform the interfacial polymerization reaction. The reaction time was set at 1 min in order to obtain the polyamide layer. The resulting membrane was washed by hexane and baked at 60 °C and then stored in DI water at 4 °C before use. The membranes were denoted as TFC-Ag1, TFC-Ag5, TFC-Ag20, and TFC-Ag100 based on the AgNPs loading condition.

Membrane Characterization. The surface morphologies of the polysulfone substrates and TFC membranes were assessed by scanning electron microscopy (SEM, LEO1530, FEG UK) at 5 kV. Before characterization, samples were dried and coated by platinum and gold. Transmission electron microscopy (TEM, Philips CM100) was used to examine the cross-sectional images of the polyamide membranes according to our previous study.[36] Briefly, membrane samples were embedded in a resin (Epon, Ted Pella, CA). After curing, the resin block was sectioned by an Ultracut E ultramicrotome (Reichert, Inc. Depew, NY) into TEM sections of 100 nm in thickness. These sections were picked up onto a copper grid and further examined in TEM at an accelerated voltage of 100 KV. Size distributions of the observed nanochannels were obtained using image analyzing software (Image-Pro Plus 6.0, MediaCybernetics, Inc). The detailed information of attenuated total reflection Fourier transform infrared (ATR-FTIR) for analyzing membrane surface functional groups, atomic force microscopy (AFM) for membrane roughness evaluation, X-ray photoelectron spectroscopy (XPS) for membrane surface elemental composition quantification, streaming potential for membrane zeta potential measurement and quartz crystal microbalance with dissipation (QCM-D) for the sorption test can be found in our previous work.[23, 27, 37]

Separation Performance Testing. Membrane water flux and solutes rejection were evaluated by a cross-flow filtration setup based on our previous method.[27] The

membrane was filtrated by DI water at an applied pressure of 21 bar for at least 3 h to achieve a stable water flux. When measuring the water flux, the pressure was reduced to 20 bar, and water flux was calculated based on Equation (1).

$$J_w = \frac{V}{A \times \Delta t} \quad (1)$$

where J_w ($Lm^{-2}h^{-1}$) is the pure water flux, V (L) is the volume of permeate, A (m^2) is the membrane area and Δt (h) is the testing time. Then, NaCl was added to the feed solution at 2000 ppm. The filtration test was continued for another 3 h and NaCl rejection (Equation (2)) was determined by measuring the conductivity of the feed and permeate solution with a conductivity meter (Ultrameter II ^{TM}, Myron Company, Carlsbad, CA).

$$R = (1 - \frac{C_p}{C_f}) \times 100\% \quad (2)$$

where R is the salt rejection, where C_p and C_f are the conductivity of the permeate and original feed solution, respectively.

The water permeability was based on Equation (3), while the salt permeability was calculated using Equation (4).[27]

$$A = \frac{J_w}{\Delta P - \Delta \pi} \quad (3)$$

$$B = \frac{1-R}{R} J_w \quad (4)$$

where A ($Lm^{-2}h^{-1}bar^{-1}$) is the membrane water permeability, $\Delta\pi$ is the difference of osmotic pressure between feed and permeate, ΔP is the applied hydraulic pressure, and B ($Lm^{-2}h^{-1}$) represents the membrane salt permeability,

To assess the membrane separation performance, we further measured the rejection of a set of neutral hydrophilic probes (ethylene glycol, diethylene glycol, and pentaerythritol), an inorganic micropollutant (boron), and organic micropollutants (propylparaben, norfloxacin, and ofloxacin). The rejection of ethylene glycol, diethylene glycol, and pentaerythritol (dosed at 200 ppm each in the feed solution) was measured at 20 bar following similar procedures of NaCl rejection measurement. Total organic carbon (TOC, Aurora 1030, OI Analytical, College Station, TX) was used to analyze the concentration of ethylene glycol, diethylene glycol, and pentaerythritol in the feed and permeate samples. The determination of Boron rejection (5 ppm, at pH 6) was similarly conducted, in which an inductive coupled plasma optical emission spectrometer (ICP-OES, Optima 8×00, PerkinElmer) was used to analyze the boron concentration.[38]

The rejection of organic micropollutants (propylparaben, norfloxacin, and ofloxacin)

was also evaluated. Following the membrane pre-compaction by DI water, a 1 mL stock solution (1 g/L) of each compound was spiked into the 5 L feed solution to form a concentration of 200 μg/L. The filtration process was then continued for another 12 h. Subsequently, samples from the feed solution and permeate were collected for further detection of these compounds using an UPLC-MS/MS system.[39] The LC separation was implented on an Agilent 1290 system (Santa Clara, CA) using an C18 column (Eclipse Plus, Agilent, 2.1 × 50 mm, 1.8 μm particle size) and the MS/MS quantification was achived using an API3200 mass detector (AB Sciex, MA).

RESULTS

Silver nanoparticles induce nanochannel formation. SEM micrographs (Figure 2, left panel) show that all the polyamide membranes had ridge-and-valley surface morphology that is often observed for RO membranes.[40, 41] FTIR results (Figure S5 in the Supporting Information) showed the characteristic peaks at 1541 cm^{-1}, 1609 cm^{-1} and 1663 cm^{-1}, representing the Amide II band, the aromatic N-H deformation vibration, and the Amide I band, respectively.[42] TEM cross-sectional images (Figure 2, right panel) also showed the rough polyamide rejection layer, which are in good agreement with the SEM observations. In addition, the TFC-Ag membranes showed increased presence of AgNPs at higher concentration of the $AgNO_3$, which is consistent with the ICP analysis (Figure S1). At relatively low AgNP loading, no severe aggregation of AgNPs occurred (e.g., see the high resolution TEM for TFC-Ag20 in Figure S7a). Nevertheless, aggregation of AgNPs became obvious for TFC-Ag100 (see its TEM cross-section in Figure 2) due to the high $AgNO_3$ used to generate the AgNPs.

Interestingly, we observed the presence of a light-colored ring around each AgNPs in the magnified TEM cross-sections of the TFC-Ag membranes (insets of Figure 2, left panel; also see Figure S7b). Such rings were not found in the control TFC membrane. In TEM micrographs, light colored region corresponds to lower mass density.[43] Therefore, we attribute the rings in the TFC-Ag membranes to the presence of

nanochannels around the AgNPs. The TEM characterization directly supports our hypothesis: the presence of hydrophilic nanoparticles induce the formation of nanochannels. In the current study, the hydrophilic AgNPs (Figure S1) could attract water molecules around them, which serves to hydrolyze TMC and terminate the interfacial polymerization in their vicinity (Figure 1a). Further analysis suggests that the size of these nanochannels was approximately 2.5 nm and was nearly independent on the silver loading (Figure S3).

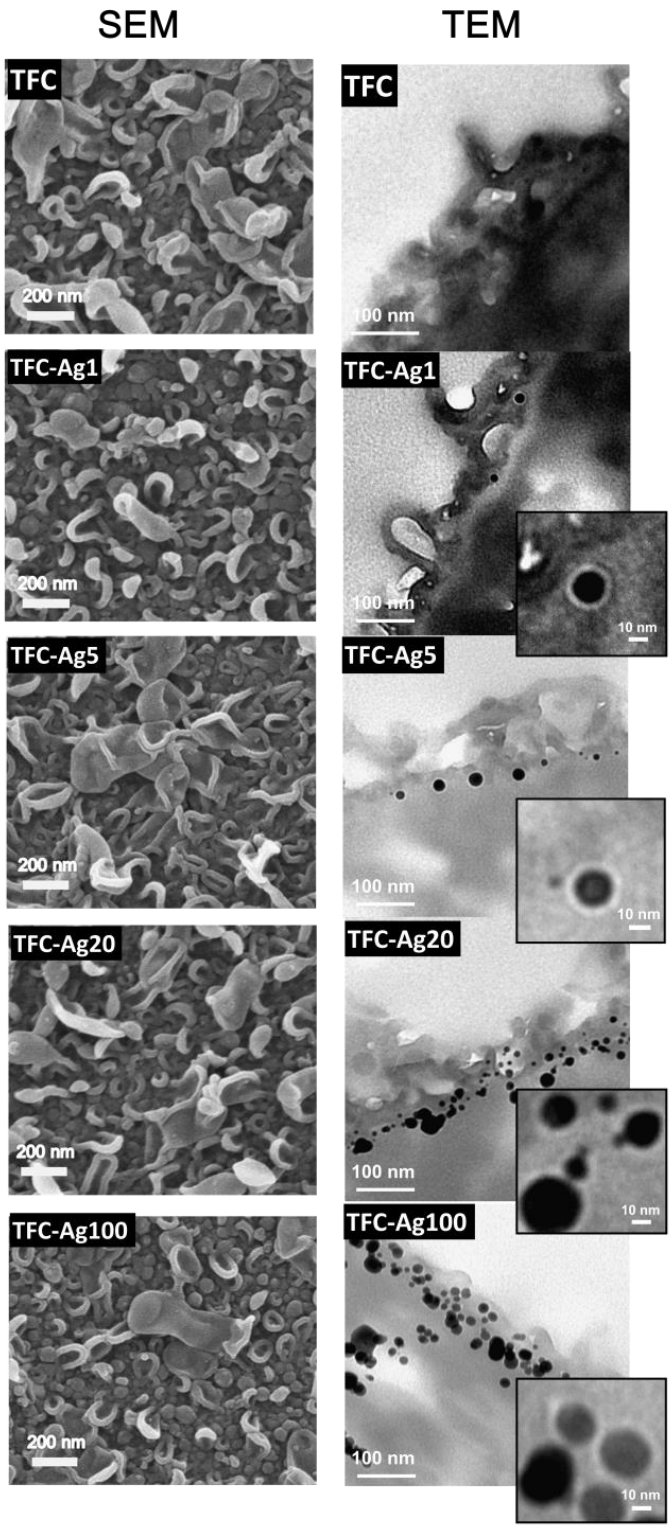

Figure 2. SEM plan view (left panel) and TEM cross-sections (right panel) of the control TFC and TFC-Ag membranes (magnified micrographs of the AgNPs nanochannels showed in the insets of the corresponding TEM images).

AgNPs-induced nanochannels enhance membrane separation performance.

Figure 3a presents the separation performance of the control and TFC-Ag membranes. With the exception of the TFC-Ag100, increasing the AgNPs loading significantly enhanced membrane water flux. Specifically, the TFC-Ag20 membrane showed the highest water flux of 50.0 ± 4.2 L $m^{-2}h^{-1}$, which was approximately 170% higher than that of the control TFC membrane (18.6 ± 2.1 L $m^{-2}h^{-1}$, Figure 3a). Such a significant enhancement can be attributed to the AgNPs-induced nanochannels, which act as shortcuts for water transport to significantly reduce membrane hydraulic resistance.[27] In addition, the hydrophilic nature of AgNPs may also be beneficial to facilitate water transport.[36] The TFC-Ag20 membrane also showed the highest NaCl rejection of 99.1 ± 0.1%, compared to that of the control TFC membrane of 97.4 ± 0.5%. In the current study, the size of the nanochannels (approximately 2.5 nm, Figure S3) was significantly larger than the hydrated size of Na^+ (0.358 nm) and Cl^- (0.270 nm).[44] Nevertheless, these nanochannels were narrower than the typical Debye length under the prevailing ionic environment (e.g., approximately 16.5 nm for a permeate water of ~20 ppm by assuming a rejection of 99%, Supporting Information S5).[45, 46] Thus, the AgNPs could play an important role in enhancing NaCl rejection due to the Donnan exclusion effect.[47] In addition, the improved NaCl rejection of TFC-Ag20 is partially attributed to its improved crosslinking (Figure 4). The presence of AgNPs enhanced the sorption of MPD on the PSF-Ag20 substrate during the interfacial polymerization stage (Figure 4a), possibly due to the synergistic effect of hydrophilic interaction and coordination between MPD and AgNPs.[48, 49] This greater MPD sorption led to

increased crosslinking degree (Figure 4b),[50] which is beneficial for improving membrane rejection by enhanced size exclusion. Overloading of AgNPs (e.g., TFC-Ag100) led to simultaneous loss of water permeability and salt rejection, potentially due to the aggregation of the AgNPs. The overlaying of AgNPs on each other (see TEM of TFC-Ag100 in Figure 2) not only increases the effective water transport path but also deteriorates the polyamide rejection layer.

We further compared the permeability and selectivity of the TFC-Ag20 membrane to TFC RO membranes reported in the recent literature (e.g., TFN,[7, 8] freestanding polyamide[51] and layer-by-layer polyamide membranes[52]) as well as representative commercial RO membranes. In Figure 3b, the TFC-Ag20 membrane exhibited both excellent water permeability and salt selectivity, exceeding the conventional permeability-selectivity trade-off.

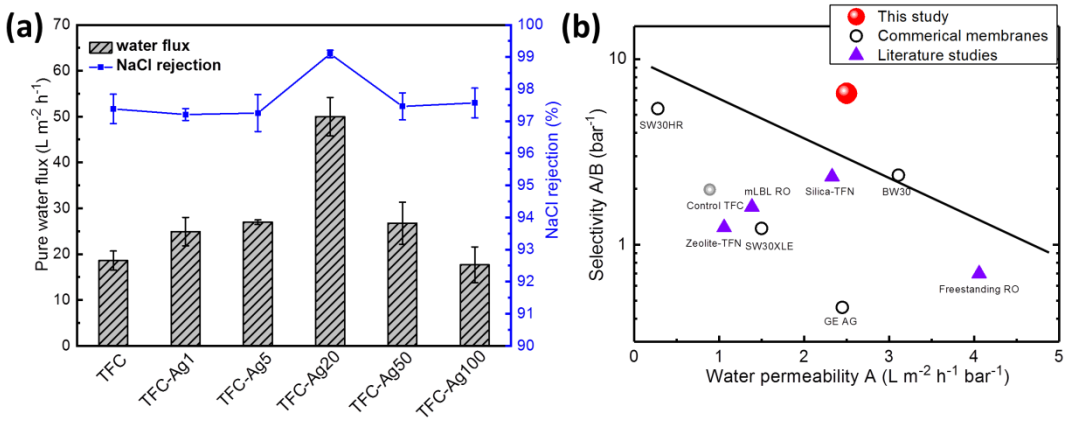

Figure 3. (a) Separation performance results of the control and TFC-Ag membranes at an applied pressure of 20 bar using 2000 ppm NaCl solution, (b) tradeoff of membrane water permeability and selectivity (water over NaCl) based on commercial membranes and literature data.[7, 8, 51, 52] The salt rejection tests for all commercial membranes and literature

data were carried out with 2000 ppm NaCl solution and their water permeability *A* values (L $m^{-2}h^{-1}bar^{-1}$) have been normalized by pressure.

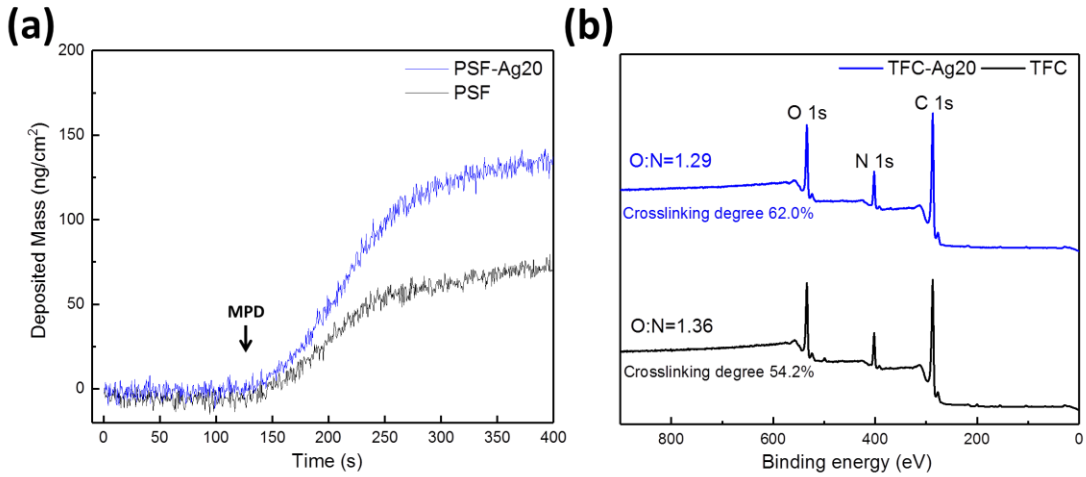

Figure 4. (a) QCM-D sorption test of MPD monomer (1 wt%) on the control and PSF-Ag20 substrates coated quartz crystal sensor, (b) XPS spectra of the control TFC and TFC-Ag20 membranes.

AgNPs-induced nanochannels enhance the rejection of organic micropollutants. Figure 5a presents the rejection of various solutes by the control and the TFC-Ag20 membrane. In this comparison, we included a salt (NaCl), a set of neutral hydrophilic solutes (boron, ethylene glycol, diethylene glycol, and pentaerythritol, norfloxacin, and ofloxacin), and a hydrophobic compound propylparaben. In all cases, the TFC-Ag20 membrane had better rejection compared to the control TFC membrane, which is partially attributed to its enhanced crosslinking degree (Figure 4b) and thus greater size exclusion effect. To gain a better understanding of the underlining mechanisms, we analyzed the selectivity enhancement factor for each compound by normalizing the respective *A*/*B* value of

304 the TFC-Ag20 membrane against that of the control membrane.[39] A higher normalized
305 *A*/*B* value indicates greater improvement in selectivity for the AgNPs-loaded
306 TFC-Ag20 membrane. Figure 5b, the data points for the neutral hydrophilic solutes
307 collapsed into a single trend line, which reveals the contribution of the improved size
308 exclusion effect.[53] In general, the enhancement factor of the TFC-Ag20 membrane
309 systematically decreased with the increased molecular weight. This is reasonable;
310 when the size of the solute is large than the pores of both membranes, the selectivity
311 enhancement factor would theoretically approach to unity (i.e., no enhancement) since
312 both membranes would completely reject the solute. Interestingly, the salt (NaCl) and
313 the hydrophobic compound (propylparaben) showed greater enhancement in
314 selectivity compared to the trend line that incorporated the effect of size exclusion.
315 This result suggests the involvement of additional mechanisms. The charged NaCl
316 benefits from the additional Donnan exclusion effect with the presence of the
317 negatively charged AgNPs (Table S1). On the other hand, the suppressed hydrophobic
318 interaction for the propylparaben (thanks to the hydrophilic nature of AgNPs), in
319 addition to its enhanced size exclusion effect, explains the greatly improved
320 selectivity of the TFC-Ag20 membrane against this hydrophobic compound.[39]
321

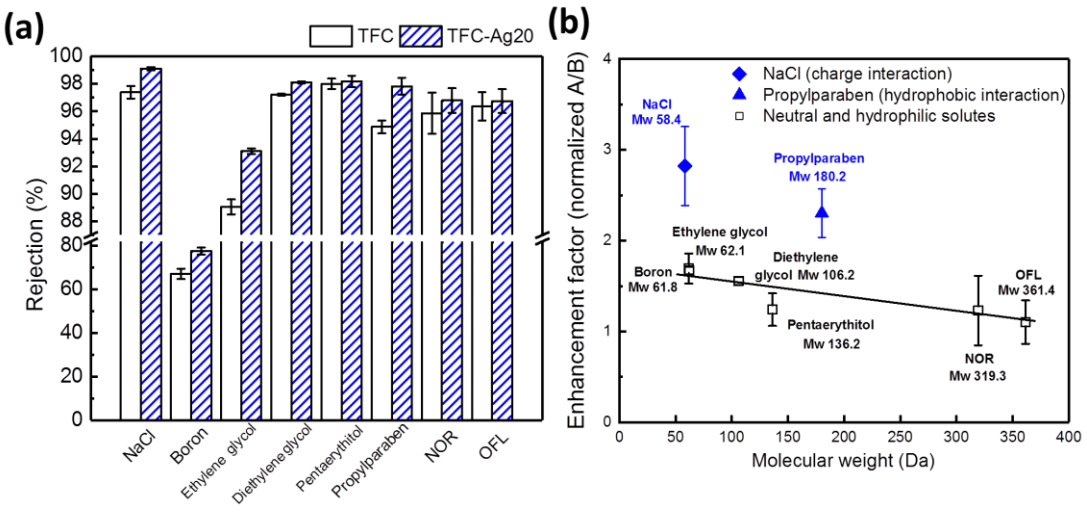

322

323 Figure 5 (a) Membrane rejection results of the control TFC and TFC-Ag20 membranes on
324 charged (NaCl), neutral (boron and diethylene glycol), hydrophobic (propylparaben) and
325 hydrophilic solutes (OFL and NOR), (b) the correlation between the molecular weight of
326 these various solutes and the enhancement factor of membrane selectivity (normalized A/B).

327

IMPLICATIONS AND PERSPECTIVES

In this study, we revealed that hydrophilic AgNPs induced the formation of nanochannels in TFN membranes, which significantly enhanced membrane water permeability. The size of the nanochannels (2-3 nm) was much narrower than the characteristic Debye length (>10 nm), leading to enhanced salt rejection due to the Donnan exclusion effect. The incorporating of AgNPs also increased the crosslinking degree of the resulting polyamide membrane for further enhanced membrane rejection and selectivity. In addition, we revealed that these nanochannels could greatly improve the removal of a hydrophobic endocrine disrupting chemical (EDC, propylparaben), thanks to the weakened hydrophobic interaction. Due to their significant health implications yet relatively poor removal of RO membranes, EDCs presents a critical challenge in the context of water reuse.[3] The current study may potentially provide a rational approach to design membranes for enhanced removal of EDCs as well as other hydrophobic micropollutants (e.g., pesticides and herbicides).

Although the current study focused on the use of AgNPs, the approach can be potentially applied to other types of nanoparticles. Table 1 summarizes recently published results for TFN membranes incorporating solid nanofillers. We categorize these TFN membranes by the phase that nanofillers are introduced (water vs. organic), the type of nanofillers, and their hydrophilicity/hydrophobicity. Incorporation of hydrophobic nanofillers during interfacial polymerization, regardless in the water or

organic phase, appeared to decrease the water permeability;[27, 28] the solid nanofillers without nanochannels around them would block the water transport and increase the membrane resistance. In contrast, the incorporation of hydrophilic nanofillers in water phase could generally result in higher water flux, which is consistent with the nanochannel formation. The corresponding salt rejection can either increase or decrease; the latter may be attributed to agglomeration of nanofillers.[32] In this regard, preloading nanofillers (e.g., by *in situ* generation of AgNPs in this study) can provide a more uniform particle loading (Figure 2) and thereby provide enhanced solute rejection. Finally, loading hydrophilic nanofillers in organic phase results in less consistent effect, with several studies[25, 54, 55] reporting reduced water permeability. Future studies need to further investigate the underlying mechanisms governing the behavior of these membranes.

Table 1. Comparison of recent solid nanomaterials incorporated TFN membranes.

Phase	Nanofiller	Hydrophilicity	Water flux	Salt rejection	Published year and Ref.	Remark
Water	AgNPs	Hydrophilic	Pw ↑ by 170%	NaCl rejection ↑	This work	Preloaded on PSF
	AgNPs		Pw ↑ by 110%	MgSO4 and NaCl rejection ↑	2017 [23]	Preloaded on PSF
	Silica		Pw ↑ by 130%	NaCl rejection ↑	2009[14]	IP
	AgNPs		Pw ↑ by 82%	MgSO4 and NaCl rejection ↓	2012[24]	IP
	Silica		Pw ↑ 150	$NaSO_4$ rejection ↗ ↘	2013[56]	IP
	TiO_2		Pw ↑ by 70%	NaCl rejection ↓	2013[55]	IP
	Na^+-CQDs[a]		Pw ↑ by 47%	NaCl rejection unchanged	2019[21]	IP
	CuNPs	Hydrophobic	Pw ↓ 50%	NaCl rejection unchanged	2018[27]	Preloaded on PSF
Organic	AgNPs	Hydrophilic	Pw slightly ↓	MgSO4 rejection ↑;	2007[25]	IP
	Silica		Pw ↑ by 30%	No change in NaCl rejection	2012[8]	IP
	TiO_2		Pw slightly ↓	MgSO4 rejection ↑	2007[54]	IP
	TiO_2		Pw slightly ↓	NaCl rejection ↑	2013[55]	IP
	Fluorinated silica	Hydrophobic	P_w ↓ 35%	NaCl rejection ↗ ↘	2017[28]	IP

ASSOCIATED CONTENT

Supporting Information

The Supporting Information is available free of charge on the ACS Publications website at DOI:

S1. SEM micrographs, silver mass density, contact angles and permeability of the control and AgNPs modified PSF substrates; S2. Size distributions of the AgNPs induced nanochannels; S3. Physiochemical properties of TFC membranes; S4. Zeta potential of AgNPs; S5. Calculation of Debye length; S6. Calculation of membrane crosslinking degree; S7. Membrane rejection of neutral hydrophilic solutes; S8. Membrane fouling behavior.

AUTHOR INFORMATION

Corresponding Author

*Phone: (+852) 2859 1976; e-mail: tangc@hku.hk

Notes

The authors declare no completing financial interest.

Acknowledgement

This study receives financial support from the Seed Funding for Strategic Interdisciplinary Research Scheme, the University of Hong Kong.

REFERENCES

1. Yang, Z.; Ma, X.-H.; Tang, C. Y., Recent development of novel membranes for desalination. *Desalination* **2018,** *434*, 37-59.
2. Elimelech, M.; Phillip, W. A., The future of seawater desalination: energy, technology, and the environment. *Science* **2011,** *333*, (6043), 712-717.
3. Tang, C. Y.; Yang, Z.; Guo, H.; Wen, J.; Nghiem, L. D.; Cornelissen, E. R., Potable water reuse through advanced membrane technology. *Environ. Sci. Technol.* **2018,** *52*, (18), 10215-10223.
4. Cohen-Tanugi, D.; McGovern, R. K.; Dave, S. H.; Lienhard, J. H.; Grossman, J. C., Quantifying the potential of ultra-permeable membranes for water desalination. *Energy Environ. Sci.* **2014,** *7*, (3), 1134-1141.
5. Geise, G. M.; Park, H. B.; Sagle, A. C.; Freeman, B. D.; McGrath, J. E., Water permeability and water/salt selectivity tradeoff in polymers for desalination. *J. Membr. Sci.* **2011,** *369*, (1), 130-138.
6. Werber, J. R.; Osuji, C. O.; Elimelech, M., Materials for next-generation desalination and water purification membranes. *Nature Review Materials* **2016,** *1*, 16018.
7. Jeong, B.-H.; Hoek, E. M.; Yan, Y.; Subramani, A.; Huang, X.; Hurwitz, G.; Ghosh, A. K.; Jawor, A., Interfacial polymerization of thin film nanocomposites: a new concept for reverse osmosis membranes. *J. Membr. Sci.* **2007,** *294*, (1), 1-7.
8. Yin, J.; Kim, E.-S.; Yang, J.; Deng, B., Fabrication of a novel thin-film nanocomposite (TFN) membrane containing MCM-41 silica nanoparticles (NPs) for water purification. *J. Membr. Sci.* **2012,** *423*, 238-246.
9. Wu, H.; Tang, B.; Wu, P., Optimizing polyamide thin film composite membrane covalently bonded with modified mesoporous silica nanoparticles. *J. Membr. Sci.* **2013,** *428*, 341-348.
10. Ma, D.; Peh, S. B.; Han, G.; Chen, S. B., Thin-Film Nanocomposite (TFN) Membranes Incorporated with Super-Hydrophilic Metal–Organic Framework (MOF) UiO-66: Toward Enhancement of Water Flux and Salt Rejection. *ACS Appl. Mater. Interfaces* **2017,** *9*, (8), 7523-7534.
11. Sorribas, S.; Gorgojo, P.; Téllez, C.; Coronas, J.; Livingston, A. G., High flux thin film nanocomposite membranes based on metal–organic frameworks for organic solvent nanofiltration. *J. Am. Chem. Soc.* **2013,** *135*, (40), 15201-15208.
12. Zhao, Y.; Qiu, C.; Li, X.; Vararattanavech, A.; Shen, W.; Torres, J.; Helix-Nielsen, C.; Wang, R.; Hu, X.; Fane, A. G., Synthesis of robust and high-performance aquaporin-based biomimetic membranes by interfacial polymerization-membrane preparation and RO performance characterization. *J. Membr. Sci.* **2012,** *423*, 422-428.
13. Qi, S.; Wang, R.; Chaitra, G. K. M.; Torres, J.; Hu, X.; Fane, A. G., Aquaporin-based biomimetic reverse osmosis membranes: Stability and long term performance. *J. Membr. Sci.* **2016,** *508*, 94-103.

14. Jadav, G. L.; Singh, P. S., Synthesis of novel silica-polyamide nanocomposite membrane with enhanced properties. *J. Membr. Sci.* **2009,** *328*, (1), 257-267.
15. Niksefat, N.; Jahanshahi, M.; Rahimpour, A., The effect of SiO2 nanoparticles on morphology and performance of thin film composite membranes for forward osmosis application. *Desalination* **2014,** *343*, 140-146.
16. Lee, H. S.; Im, S. J.; Kim, J. H.; Kim, H. J.; Kim, J. P.; Min, B. R., Polyamide thin-film nanofiltration membranes containing TiO2 nanoparticles. *Desalination* **2008,** *219*, (1-3), 48-56.
17. Rajaeian, B.; Rahimpour, A.; Tade, M. O.; Liu, S., Fabrication and characterization of polyamide thin film nanocomposite (TFN) nanofiltration membrane impregnated with TiO2 nanoparticles. *Desalination* **2013,** *313*, 176-188.
18. Li, H.; Shi, W.; Zhu, H.; Zhang, Y.; Du, Q.; Qin, X. J. F.; Polymers, Effects of zinc oxide nanospheres on the separation performance of hollow fiber poly (piperazine-amide) composite nanofiltration membranes. *Fiber. Polym.* **2016,** *17*, (6), 836-846.
19. Balta, S.; Sotto, A.; Luis, P.; Benea, L.; Van der Bruggen, B.; Kim, J., A new outlook on membrane enhancement with nanoparticles: the alternative of ZnO. *J. Membr. Sci.* **2012,** *389*, 155-161.
20. Wang, Y.; Gao, B.; Li, S.; Jin, B.; Yue, Q.; Wang, Z. J. C., Cerium oxide doped nanocomposite membranes for reverse osmosis desalination. *Chemosphere* **2018,** *218*, 974-983.
21. Gai, W.; Zhao, D. L.; Chung, T.-S., Thin film nanocomposite hollow fiber membranes comprising Na+-functionalized carbon quantum dots for brackish water desalination. *Water Res.* **2019,** *154*, 54-61.
22. Zhao, D. L.; Chung, T.-S., Applications of carbon quantum dots (CQDs) in membrane technologies: A review. *Water Res.* **2018,** *147*, 43-49.
23. Yang, Z.; Wu, Y.; Guo, H.; Ma, X.-H.; Lin, C.-E.; Zhou, Y.; Cao, B.; Zhu, B.-K.; Shih, K.; Tang, C. Y., A novel thin-film nano-templated composite membrane with in situ silver nanoparticles loading: Separation performance enhancement and implications. *J. Membr. Sci.* **2017,** *544*, 351-358.
24. Kim, E.-S.; Hwang, G.; Gamal El-Din, M.; Liu, Y., Development of nanosilver and multi-walled carbon nanotubes thin-film nanocomposite membrane for enhanced water treatment. *J. Membr. Sci.* **2012,** *394-395*, 37-48.
25. Lee, S. Y.; Kim, H. J.; Patel, R.; Im, S. J.; Kim, J. H.; Min, B. R., Silver nanoparticles immobilized on thin film composite polyamide membrane: characterization, nanofiltration, antifouling properties. *Polym. Adv. Technol.* **2007,** *18*, (7), 562-568.
26. Lau, W.; Gray, S.; Matsuura, T.; Emadzadeh, D.; Chen, J. P.; Ismail, A., A review on polyamide thin film nanocomposite (TFN) membranes: History, applications, challenges and approaches. *Water Res.* **2015,** *80*, 306-324.
27. Yang, Z.; Huang, X.; Ma, X.-h.; Zhou, Z.-w.; Guo, H.; Yao, Z.; Feng, S.-P.; Tang, C. Y., Fabrication of a novel and green thin-film composite membrane containing

nanovoids for water purification. *J. Membr. Sci.* **2019,** *570-571*, 314-321.
28. Pang, R.; Zhang, K., Fabrication of hydrophobic fluorinated silica-polyamide thin film nanocomposite reverse osmosis membranes with dramatically improved salt rejection. *J. Colloid. Interface Sci.* **2018,** *510*, 127-132.
29. Chae, H.-R.; Lee, J.; Lee, C.-H.; Kim, I.-C.; Park, P.-K., Graphene oxide-embedded thin-film composite reverse osmosis membrane with high flux, anti-biofouling, and chlorine resistance. *J. Membr. Sci.* **2015,** *483*, 128-135.
30. Yin, J.; Zhu, G.; Deng, B., Graphene oxide (GO) enhanced polyamide (PA) thin-film nanocomposite (TFN) membrane for water purification. *Desalination* **2016,** *379*, 93-101.
31. Yang, Z.; Yin, J.; Deng, B., Enhancing water flux of thin-film nanocomposite (TFN) membrane by incorporation of bimodal silica nanoparticles. *Aims Press Envrion. Sci.* **2016,** *3*, (2), 185-198.
32. Yin, J.; Deng, B., Polymer-matrix nanocomposite membranes for water treatment. *J. Membr. Sci.* **2015,** *479*, 256-275.
33. Cataliotti, R. S.; Aliotta, F.; Ponterio, R., Silver nanoparticles behave as hydrophobic solutes towards the liquid water structure in the interaction shell. A Raman study in the O–H stretching region. *Phys. Chem. Chem. Phys.* **2009,** *11*, (47), 11258-11263.
34. Ma, X.-H.; Yang, Z.; Yao, Z.-K.; Xu, Z.-L.; Tang, C. Y., A facile preparation of novel positively charged MOF/chitosan nanofiltration membranes. *J. Membr. Sci.* **2017,** *525*, 269-276.
35. Ben-Sasson, M.; Lu, X.; Bar-Zeev, E.; Zodrow, K. R.; Nejati, S.; Qi, G.; Giannelis, E. P.; Elimelech, M., In situ formation of silver nanoparticles on thin-film composite reverse osmosis membranes for biofouling mitigation. *Water Res.* **2014,** *62*, 260-70.
36. Yang, Z.; Wu, Y.; Wang, J.; Cao, B.; Tang, C. Y., In situ reduction of silver by polydopamine: A novel antimicrobial modification of a thin-film composite polyamide membrane. *Environ. Sci. Technol.* **2016,** *50*, (17), 9543-50.
37. Yang, Z.; Zhou, Z. W.; Guo, H.; Yao, Z.; Ma, X. H.; Song, X.; Feng, S. P.; Tang, C. Y., Tannic Acid/Fe(3+) Nanoscaffold for Interfacial Polymerization: Toward Enhanced Nanofiltration Performance. *Environ. Sci. Technol.* **2018,** *52*, (16), 9341-9349.
38. Hu, J.; Pu, Y.; Ueda, M.; Zhang, X.; Wang, L., Charge-aggregate induced (CAI) reverse osmosis membrane for seawater desalination and boron removal. *J. Membr. Sci.* **2016,** *520*, 1-7.
39. Guo, H.; Deng, Y.; Yao, Z.; Yang, Z.; Wang, J.; Lin, C.; Zhang, T.; Zhu, B.; Tang, C. Y., A highly selective surface coating for enhanced membrane rejection of endocrine disrupting compounds: Mechanistic insights and implications. *Water Res.* **2017,** *121*, 197-203.
40. Ma, X.-H.; Yao, Z.; Yang, Z.; Guo, H.; Xu, Z.; Tang, C. Y.; Elimelech, M., Nanofoaming of Polyamide Desalination Membranes to Tune Permeability and

Selectivity. *Environ. Sci. Technol. Lett.* **2018,** *5*, (2), 123-130.
41. Ma, X.; Yang, Z.; Yao, Z.; Guo, H.; Xu, Z.; Tang, C. Y., Tuning roughness features of thin film composite polyamide membranes for simultaneously enhanced permeability, selectivity and anti-fouling performance. *J. Colloid. Interface Sci.* **2019,** *540*, 382-388.
42. Tang, C. Y.; Kwon, Y.-N.; Leckie, J. O., Effect of membrane chemistry and coating layer on physiochemical properties of thin film composite polyamide RO and NF membranes: I. FTIR and XPS characterization of polyamide and coating layer chemistry. *Desalination* **2009,** *242*, (1-3), 149-167.
43. Tang, C. Y.; Yang, Z., Chapter 8 - Transmission Electron Microscopy (TEM). In *Membrane Characterization*, Hilal, N.; Ismail, A. F.; Matsuura, T.; Oatley-Radcliffe, D., Eds. Elsevier: 2017; pp 145-159.
44. Cheng, W.; Liu, C.; Tong, T.; Epsztein, R.; Sun, M.; Verduzco, R.; Ma, J.; Elimelech, M. J. J. o. M. S., Selective removal of divalent cations by polyelectrolyte multilayer nanofiltration membrane: Role of polyelectrolyte charge, ion size, and ionic strength. *J. Membr. Sci.* **2018,** *559*, 98-106.
45. Tang, C. Y.; Kwon, Y.-N.; Leckie, J. O., The role of foulant–foulant electrostatic interaction on limiting flux for RO and NF membranes during humic acid fouling—Theoretical basis, experimental evidence, and AFM interaction force measurement. *J. Membr. Sci.* **2009,** *326*, (2), 526-532.
46. Pfeiffer, C.; Rehbock, C.; Hühn, D.; Carrillo-Carrion, C.; de Aberasturi, D. J.; Merk, V.; Barcikowski, S.; Parak, W. J. J. J. o. T. R. S. I., Interaction of colloidal nanoparticles with their local environment: the (ionic) nanoenvironment around nanoparticles is different from bulk and determines the physico-chemical properties of the nanoparticles. *J. Royal Soc. Interface* **2014,** *11*, (96), 20130931.
47. Seidel, A.; Waypa, J. J.; Elimelech, M. J. E. E. S., Role of charge (Donnan) exclusion in removal of arsenic from water by a negatively charged porous nanofiltration membrane. *Environ. Eng. Sci.* **2001,** *18*, (2), 105-113.
48. Li, X.-G.; Ma, X.-L.; Sun, J.; Huang, M.-R., Powerful Reactive Sorption of Silver(I) and Mercury(II) onto Poly(o-phenylenediamine) Microparticles. *Langmuir* **2009,** *25*, (3), 1675-1684.
49. Chai, L.; Wang, T.; Zhang, L.; Wang, H.; Yang, W.; Dai, S.; Meng, Y.; Li, X. J. C., A Cu–m-phenylenediamine complex induced route to fabricate poly (m-phenylenediamine)/reduced graphene oxide hydrogel and its adsorption application. *Carbon* **2015,** *81*, 748-757.
50. Wei, J.; Liu, X.; Qiu, C.; Wang, R.; Tang, C. Y., Influence of monomer concentrations on the performance of polyamide-based thin film composite forward osmosis membranes. *J. Membr. Sci.* **2011,** *381*, (1-2), 110-117.
51. Jiang, Z.; Karan, S.; Livingston, A. G., Water transport through ultrathin polyamide nanofilms used for reverse osmosis. *Adv. Mater.* **2018,** *30*, (15), 1705973.
52. Gu, J. E.; Lee, S.; Stafford, C. M.; Lee, J. S.; Choi, W.; Kim, B. Y.; Baek, K. Y.; Chan, E. P.; Chung, J. Y.; Bang, J.; Lee, J. H., Molecular layer-by-layer assembled

552 thin-film composite membranes for water desalination. *Adv. Mater.* **2013,** *25*, (34),
553 4778-82.
554 53. Yang, L.; She, Q.; Wan, M. P.; Wang, R.; Chang, V. W.-C.; Tang, C. Y.,
555 Removal of haloacetic acids from swimming pool water by reverse osmosis and
556 nanofiltration. *Water Res.* **2017,** *116*, 116-125.
557 54. Lee, H. S.; Im, S. J.; Kim, J. H.; Kim, H. J.; Kim, J. P.; Min, B. R. J. D.,
558 Polyamide thin-film nanofiltration membranes containing TiO2 nanoparticles.
559 *Desalination* **2008,** *219*, (1-3), 48-56.
560 55. Rajaeian, B.; Rahimpour, A.; Tade, M. O.; Liu, S. J. D., Fabrication and
561 characterization of polyamide thin film nanocomposite (TFN) nanofiltration
562 membrane impregnated with TiO2 nanoparticles. *Desalination* **2013,** *313*, 176-188.
563 56. Hu, D.; Xu, Z.-L.; Wei, Y.-M., A high performance silica–fluoropolyamide
564 nanofiltration membrane prepared by interfacial polymerization. *Sep. Purif. Technol.*
565 **2013,** *110*, 31-38.
566